Nonlinear Analysis: Modelling and Control, Vol. 25, No. 6, 1035–1058
https://doi.org/10.15388/namc.2020.25.20563

ISSN: 1392-5113
eISSN: 2335-8963

Analysis of a model for waterborne diseases with Allee effect on bacteria*

Florinda Capone[a], **Maria Francesca Carfora**[b], **Roberta De Luca**[a], **Isabella Torcicollo**[b]

[a]Dipartimento di Matematica ed Applicazioni "R. Caccioppoli",
Universitá di Napoli Federico II,
Via Cintia, Naples, Italy
fcapone@unina.it; roberta.deluca@unina.it

[b]Istituto per le Applicazioni del Calcolo "Mauro Picone", CNR,
Via P. Castellino 111, Naples, Italy
f.carfora@iac.cnr.it; i.torcicollo@iac.cnr.it

Received: November 15, 2019 / **Revised:** October 1, 2020 / **Published online:** November 1, 2020

Abstract. A limitation of current modeling studies in waterborne diseases (one of the leading causes of death worldwide) is that the intrinsic dynamics of the pathogens is poorly addressed, leading to incomplete, and often, inadequate understanding of the pathogen evolution and its impact on disease transmission and spread. To overcome these limitations, in this paper, we consider an ODEs model with bacterial growth inducing Allee effect. We adopt an adequate functional response to significantly express the shape of indirect transmission. The existence and stability of biologically meaningful equilibria is investigated through a detailed discussion of both backward and Hopf bifurcations. The sensitivity analysis of the basic reproduction number is performed. Numerical simulations confirming the obtained results in two different scenarios are shown.

Keywords: waterborne disease, Allee effect, stability, ODEs system.

1 Introduction

Mortality from infectious diseases is still high worldwide; even if it has declined in high-income countries, it represents a crucial issue in low-income countries. A fundamental property of infectious diseases, including diseases caused by waterborne pathogens, is that these complex interactions always result from an infectious individual or environmental source transmitting the pathogen to a susceptible individual. Examples of diseases in common waterborne infections include Cholera, Giardia, Cryptosporidium, Campylobacter, Typhoid and Paratyphoid fevers, hepatitis A and E, norovirus, rotavirus and many

*This research has been performed under the auspices of the G.N.F.M. and G.N.C.S. of INdAM. Carfora and Torcicollo have been partially supported by Regione Campania Projects ADVISE and REMIAM.

others [1]; these can be caused by a variety of pathogenic microbes (bacteria, protozoa, etc.) in contaminated water. Unfortunately, waterborne diseases remain a serious public health concern today, resulting in more than 3.4 million deaths a year according to WHO estimates. Severe waterborne disease outbreaks continue to occur such as Cholera in Haiti from October 2010 to January 2014; the Zimbabwe Cholera epidemic from August 2008 to July 2009. Several different factors must be considered in attempting to understand waterborne disease dynamics including different transmission pathways such as the ingestion of contaminated water or food or consumption and use of fecally contaminated water. Due to their huge impact on public health and social and economic development, waterborne diseases have been the subject of extensive studies in clinical, experimental and theoretical fields. A number of different approaches (mathematical modeling, analysis, simulation) have been used for modeling the disease transmission, and a large number of mathematical models have been published [10, 12, 20, 21, 24]. Such models provide challenges and ideas in many other fields of applied mathematics such as ecology, economics in which nonlinear mathematical models having a similar structure are considered [2–5, 22, 23, 25]. The mathematical models allow to obtain an estimate for the behavior of epidemics and to predict the asymptotic behavior of infection in order to take suitable actions to control epidemics. On introducing a few number of infected in a population of susceptible individuals, the question that arises is if the epidemic will persist or die out. To this aim, the stability of the *disease-free equilibrium* (i.e. the equilibrium with no infection) and of the *endemic equilibria* (i.e. equilibria with nonnull population components) are analyzed. In particular: if the disease-free equilibrium is stable, then epidemic will decay; if endemic equilibria exist and are stable, then epidemic will persist. A limitation of current modeling studies in waterborne diseases, however, is that the intrinsic dynamics of the waterborne pathogens are poorly addressed, leading to incomplete, and often, inadequate, understanding of the pathogen evolution and its impact on disease transmission and spread. Most cholera models in the literature are based on the standard assumption that the pathogens cannot sustain themselves in the absence of human contribution. The rate of change for the bacterial density, in this case, is simply the sum of a positive contribution from the infected human population and a negative contribution due to natural death of the bacteria, and both contributions are assumed as linear. But there have been strong empirical evidences that the pathogens "can independently persist in the environment and, consequently, their intrinsic growth and decay may play an essential role in shaping cholera epidemics" (see [28] and further references therein). Studies from a few research groups, however [14, 27], have considered that the interaction between the pathogen and the host could be more complicated than linear. Also, the bacterial growth outside of human hosts does not have to follow linear dynamics; all the cited literature assumes more general (nonlinear) functional forms for the bacterial growth. Moreover, many recent works on the impact of climate change on the pathogens growth in relation to waterborne diseases (see the two review articles [16, 17]) suggest evidence for such nonlinear models. Richer models could be more adequate in representing such complex phenomena. Recently, a modified model describing the transmission dynamics of a waterborne bacterial infection, which sheds light on the importance of the type of intrinsic bacterial dynamics into the pathogen evolution equation, has been proposed

in [29]. The authors incorporate both direct (human-to-human) and indirect (environment-to-human) transmission pathways, each represented by a bilinear incidence, and examine two types of bacterial intrinsic dynamics: a logistic growth and a cubic growth. In all studies concerning Allee effects in microbial populations [15], a minimal density (the "Allee threshold") is needed to initiate positive population development. Moreover, to better express the shape of indirect transmission, we adopt a nonlinear function (Holling type II functional response) for the incidence [6, 10, 19]. Such a choice implies that there must be the ingestion of a certain amount of bacteria to contract the infection. These modeling assumptions highlight more interesting and complicated dynamics. In [28], a general function (depicting also the Holling type II functional) has already been considered to express the indirect transmission, but that model simply excludes the logistic growth with a threshold that we analyze in the present paper. The plan of the paper is the following. In Section 2, the mathematical model is introduced, and the basic reproduction number is recovered. The existence and uniqueness of biologically meaningful equilibria is investigated in Section 3. The linear stability analysis of the disease-free equilibrium and of the endemic equilibria (when they exist) is performed in Section 4. In Sections 5.1 and 5.2, respectively, the possible occurrence of backward/forward and Hopf bifurcations is investigated. Section 6 deals with the sensitivity analysis, while numerical simulations on the obtained results are shown in Section 7, and concluding remarks are given in Section 8.

2 Mathematical model

The model governing a waterborne disease transmission with cubic growth for the bacteria, assuming a Holling type II force of infection, is

$$\dot{S} = \mu N_0 - \beta\lambda(B)S - \mu S, \tag{1}$$

$$\dot{I} = \beta\lambda(B)S - (\mu + \delta)I, \tag{2}$$

$$\dot{B} = rB(B-b)\left(1 - \frac{B}{k}\right) + \xi I - \tau B, \tag{3}$$

$$\dot{R} = \delta I - \mu R, \tag{4}$$

where the variables $S(t)$, $I(t)$, $R(t)$ denote, respectively, the susceptible, infective and removed individuals, while $B(t)$ denotes the concentration of bacteria in contaminated water, and "$\cdot$" denotes the time derivative. The cubic growth for the bacteria is essential to induce an Allee effect experimentally demonstrated in many microbial populations [15]. The probability to catch the infection [6, 28] is $\lambda(B) = B/(K_B + B)$, being K_B (cells/ml) the constant indicating the half saturation rate. The constants appearing in (1)–(4) are positive, and for their biological meaning, we refer to Table 1.

We append to (1)–(4) smooth positive initial data

$$S(0) = S_0, \qquad I(0) = I_0, \qquad R(0) = R_0, \qquad B(0) = B_0.$$

Table 1. Description of the constants appearing in (1)–(4).

Symbols	Description	Units
N_0	total population size at time $t = 0$	person
μ	birth/death rate	t^{-1}
δ	removed rate	t^{-1}
r	bacterial intrinsic growth rate	ml cells^{-1} t^{-1}
k	carrying capacity	cells ml^{-1}
τ	bacterial removal rate	t^{-1}
$\xi = p/W$	contribution of each infected person to the population of bacteria	cells/ml t^{-1} person^{-1}
p	rate at which bacteria are produced by an infected individual	cells t^{-1} person^{-1}
W	volume of contaminated water in infected individual	ml
β	contact rate with contaminated water	t^{-1}
$b\,(< k)$	Allee threshold when $\tau = 0$	cells ml^{-1}

Setting $N(t) = S(t) + I(t) + R(t)$ the total host population size at time t, by adding (1), (2) and (4), it turns out that $\dot{N} + \mu N = \mu N_0$, and hence

$$N(t) = N_0 \quad \forall t \geqslant 0 \tag{5}$$

i.e. the total host population size is constant. From (5) it follows that each component of the host population is bounded by N_0 and $R(t) = N_0 - [S(t) + I(t)]$.

We remark that the cubic growth of bacteria induces an Allee effect on the bacteria. In fact, setting $f(B) = rB(B - b)(1 - B/k) - \tau B$, $f(B) = 0 \Leftrightarrow B = 0$ and $\lim_{B\to\infty} f(B) = -\infty$. If $\tau > r(k - b)^2/(4k)$, then $f(B)$ is negative definite for $B \in]0, \infty[$. Then, from (3), it turns out that $B(t)$ goes into extinction in the absence of infected individuals (i.e. bacteria population can not sustain itself in the absence of infected individuals). If

$$\tau < \frac{r(k - b)^2}{4k}, \tag{6}$$

then there exist two positive constants $b_1 = (r(k+b) - \sqrt{r^2(k-b)^2 - 4kr\tau})/(2r)$, $k_1 = (r(k+b) + \sqrt{r^2(k-b)^2 - 4kr\tau})/(2r)$ such that, in the absence of infected individuals: (i) if $B(t) < b_1$, then $B(t)$ goes into extinction; (ii) if $b_1 < B(t) < k_1$, then $B(t)$ exponentially increases up to k_1; (iii) if $B(t) > k_1$, then $B(t)$ exponentially decreases up to k_1. In this sense, b_1 and k_1 represent the Allee threshold and the carrying capacity, respectively. Since we are interested in the case in which bacteria can sustain themselves even in the absence of infected individuals, in the sequel, we assume that (6) holds.

Model (1)–(4) admits the (unique) disease-free equilibrium $E_0 = (N_0, 0, 0, 0)$. By using the next generation method [26], we determine the basic reproduction number $\mathcal{R}_0$ defined as "the expected number of secondary cases produced by a typical infected individual during its entire period of infectiousness in a completely susceptible population" [11]. I and B are the only compartments directly related to the disease. The matrices denoting the generation of new infections and the transfer among infectious compartments are, respectively, given by

$$F = \begin{pmatrix} 0 & \beta N_0/K_B \\ \xi & 0 \end{pmatrix}, \qquad V = \begin{pmatrix} \mu + \delta & 0 \\ 0 & rb + \tau \end{pmatrix},$$

then the basic reproduction number is given by

$$\mathcal{R}_0 = \rho\big(FV^{-1}\big) = \frac{\beta N_0 \xi}{K_B(\mu+\delta)(\tau+rb)}.$$

3 Nontrivial equilibria

In this section, we determine the equilibria of (1)–(4) having all positive components. A nontrivial equilibrium is a solution of the system

$$\mu N_0 = \beta\lambda(B)S + \mu S, \tag{7}$$

$$\beta\lambda(B)S = (\mu+\delta)I, \tag{8}$$

$$\xi I = rB(b-B)\left(1-\frac{B}{k}\right) + \tau B, \tag{9}$$

$$\delta I - \mu R = 0 \tag{10}$$

given by

$$\bar{S} = N_0 - \frac{\bar{B}(\delta+\mu)[-(\bar{B}-b)(1-\frac{\bar{B}}{k})r+\tau]}{\mu\xi},$$

$$\bar{I} = \frac{\bar{B}[-(\bar{B}-b)(1-\frac{\bar{B}}{k})r+\tau]}{\xi}, \qquad \bar{R} = \frac{\delta\bar{B}[-(\bar{B}-b)(1-\frac{\bar{B}}{k})r+\tau]}{\mu\xi},$$

being $\bar{B} > 0$ a positive root of the equation

$$Q(B) := A_1B^3 + A_2B^2 + A_3B + A_4 = 0, \tag{11}$$

where

$$\begin{aligned} &A_1 = r(\beta+\mu)(\delta+\mu) > 0, \qquad A_2 = -r(\delta+\mu)\big(-K_B\mu + (k+b)(\beta+\mu)\big),\\ &A_3 = (\delta+\mu)\big[-kK_Br\mu + br\big(-K_B\mu + k(\beta+\mu)\big) + k(\beta+\mu)\tau\big],\\ &A_4 = k\mu\big[-N_0\beta\xi + K_B(\delta+\mu)(br+\tau)\big] = k\mu K_B(\delta+\mu)(br+\tau)(1-R_0). \end{aligned} \tag{12}$$

Let us investigate how many equilibria are admitted by system (7)–(10). Setting $\theta = \mu N_0/(\mu+\delta)$, from (7) and (8) it follows that

$$I = \frac{\theta\beta B}{\beta B + \mu(K_B+B)} := g(B), \tag{13}$$

$$B = \frac{\mu K_B I}{\theta\beta - (\beta+\mu)I} = p(I).$$

From (9) it follows that

$$I = \frac{rB}{\xi k}\left[B^2 - (k+b)B + \frac{k}{r}(\tau+rb)\right] := q(B), \tag{14}$$

and in view of the positiveness of I, when (6) holds, it provides the following necessary condition for the existence of a nontrivial equilibrium:

$$0 < B < b_1 \quad \text{or} \quad B > k_1. \tag{15}$$

In order to find nontrivial equilibria, from (13) and (14) one has to solve

$$g(B) = q(B), \quad B > 0.$$

The following theorem holds.

Theorem 1. *If* (6) *holds true, then*

- $\mathcal{R}_0 < 1$ *implies that there exist* 2 *endemic equilibria*;
- $\mathcal{R}_0 = 1$ *implies that there exist* 1 *or* 2 *endemic equilibria*;
- $\mathcal{R}_0 > 1$ *implies that there exist* 1, 2 *or* 3 *endemic equilibria.*

Proof. Let us start by remarking that $g(B) > 0$ for all $B > 0$, while $q(B) > 0$ if and only if (15) holds. Furthermore,

$$g'(B) = \frac{\mu K_B \theta\beta}{[\beta B + \mu(K_B + B)]^2} > 0, \qquad g''(B) = -\frac{2\mu K_B \theta\beta(\mu+\beta)}{[\beta B + \mu(K_B + B)]^3} < 0,$$
$$q'(B) = \frac{r}{\xi k}\left[3B^2 - 2(b+k)B + \frac{k}{r}(\tau + br)\right].$$

1.1. Nontrivial equilibria in the case $B > k_1$. Let us analyze the case $\tau < r(k-b)^2/(4k)$, $B > k_1$. In this case, $q'(B) \geqslant 0 \Leftrightarrow B < B_1$, $B > B_2$, where $B_{1,2} = (b+k \pm \sqrt{(b+k)^2 - 3k(\tau+br)/r})/3$ and $q''(B) > 0 \Leftrightarrow B > (b+k)/3$. Simple calculation shows that $B_2 < k_1$. Hence, when $B > k_1$, $q(B)$ is an increasing, convex function of B that crosses $g(B)$ in one point. For this reason, in this case, there exists a unique nontrivial equilibrium.

1.2. Nontrivial equilibria in the case $B < b_1$. Let us analyze the case $\tau < r(k-b)^2/(4k)$, $B < b_1$. Setting $T(B) = q(B) - g(B)$, $T(B) = B\{(r/\xi k)[B^2 - (b+k)B + (k/r)(\tau+rb)] - \theta\beta/(\beta B + \mu(K_B+B))\}$, we look for the positive solutions of $T(B) = 0$. Let us remark that

$$T(0) = 0, \qquad T(b_1) = q(b_1) - g(b_1) = -g(b_1) < 0,$$
$$T'(B) = \frac{r}{\xi k}\left[3B^2 - 2(b+k)B + \frac{k}{r}(\tau + rb)\right] - \frac{\theta\mu\beta K_B}{[\beta B + \mu(K_B+B)^2]}.$$

Hence, $T'(0) = (\tau + rb)(1 - \mathcal{R}_0)/\xi$, $T'(b_1) = [2b_1 - (b+k)]rb_1/(\xi k) - g'(b_1) < 0$. Let us distinguish three cases:

1. $\mathcal{R}_0 < 1$. In this case, $T'(0) > 0$ and $T(B) = 0$ admits at least one positive root $\bar{B} \in (0, b_1)$. Let us prove that this root is unique. First, $T^{(\mathrm{iv})}(B) = -g^{(\mathrm{iv})}(B) > 0$, i.e. T'' is a convex function of B and has at most two zeros.
   - If $T''(B)$ has no zeros, then $T'(B)$ is monotone. But, since $T'(0) > 0$ and $T'(b_1) < 0$, $T'(B)$ is monotone decreasing and admits a unique solution in $(0, b_1)$;
   - If $T''(B)$ has a unique root $y \in (0, b_1)$, then $T'(B)$ is monotone in $(0, y)$ and in (y, b_1). It follows that $T'(B)$ has at most one zero in $(0, y)$ and one zero in

(y, b_1). But, since $T'(0) > 0$ and $T'(b_1) < 0$, there cannot be two solutions of $T'(B) = 0$ in $(0, b_1)$;

- If $T''(B)$ has two solutions in $(0, b_1)$, say y_1 and y_2. Let us assume that $0 < y_1 < y_2 < b_1$. One has that $T''(B) > 0$ in $(0, y_1)$, $T''(B) < 0$ in (y_1, y_2) and $T''(B) > 0$ in (y_2, b_1). Then $T'(B)$ has only one root in $(0, b_1)$; being T increasing, $T(B)$ has only one root in $(0, b_1)$.

Since $T'(B)$ has only one root in $(0, b_1)$ and T is increasing, $T(B)$ has only one root in $(0, b_1)$.

2. If $\mathcal{R}_0 = 1$, then $T(0) = 0, T(b_1) < 0, T'(0) = 0, T'(b_1) < 0, T^{(\mathrm{iv})}(B) > 0$.
   - If $T^{(n)}(0) \leqslant 0$, since $T''(B)$ is convex, there exists a unique $y > 0$ such that $T''(y) = 0$ and $T''(B) < 0$ in $(0, y)$, while $T''(B) > 0$ in (y, ∞). If $y < b_1$, then $T'(B)$ decreases in $(0, y)$ and increases in (y, b_1). Consequently, since $T'(0) = 0, T'(b_1) < 0$, $T(B)$ is decreasing in $(T(0), T(b_1))$. If $y \geqslant b_1$, $T'(B)$ is decreasing in $(0, b_1)$ and, since $T'(b_1) < T'(0) = 0$, $T'(B) < 0$, i.e. $T(B)$ is negative definite in $(0, b_1)$.
   - If $T''(0) > 0$, then $T''(B)$ has at most two zeros in $(0, b_1)$. Let us prove that $T(B)$ has a unique root. In fact, if $T''(B)$ has no roots in $(0, b_1)$, then $T''(B) > 0$ in $(0, b_1)$, i.e. $T'(B)$ is strictly increasing in $(0, b_1)$, but this is in contradiction since $T'(b_1) < 0$ and $T'(0) = 0$. If T'' has one root $y \in (0, b_1)$, then $T(B)$ is convex in $(0, y)$ and concave in (y, b_1). Since $T(y) > T(0) = 0$, $T(B)$ has one zero in $(0, b_1)$. Finally, if $T''(B)$ has two zeros in $(0, b_1)$, we can follow the procedure used in the case $R_0 < 1$ to conclude that $T(B)$ has only one root in $(0, b_1)$.
3. If $\mathcal{R}_0 > 1$, it follows that $T'(0) < 0$. By fixing all the parameters, except for the intrinsic growth rate of the bacteria, r, $g(B)$ does not vary with r, while $\partial q(B)/\partial r = B\{1/(\xi k)[B^2 - (b + k)B + kb + (k/\tau)r] - (k^2\tau)/(\xi r)\}$. Hence, if $B < b_1$, then $B^2 - (b + k)B + kb + k\tau/r > 0$, i.e. $q(B)$ (and $T(B)$) can be increasing or decreasing with r. In this case, $T(B)$ can have 0 or 1 or 2 roots in $(0, b_1)$.

In conclusion, if (6) holds, there exist a unique endemic equilibrium for $B > k_1$ for all $\mathcal{R}_0$, while there exist 0, 1 or 2 endemic equilibria for $B < b_1$ according to specific values of $\mathcal{R}_0$, and the thesis is reached.

The first thesis of Theorem 1 indicates the possible existence of backward bifurcation. We will investigate it in Section 5. □

The following sufficient condition ensures the uniqueness of the endemic equilibrium.

Theorem 2. *If* (6) *holds true and*

$$\mathcal{R}_0 > 1, \tag{16}$$

$$K_B > \frac{(k + b)(\beta + \mu)}{\mu}, \tag{17}$$

then there exists a unique endemic equilibrium.

Proof. By considering the coefficients (12), $A_1 > 0$. Moreover, (16)–(17) yields $A_4 < 0$ and $A_2 > 0$. It is then sufficient to observe that (17) along with (6) yields $A_3 < 0$. By applying Descartes' rule of signs to $Q(B)$ the thesis is reached. □

4 Linear stability of the biologically meaningful equilibria

Let $\bar{S}$, $\bar{I}$, $\bar{B}$, $\bar{R}$ be a generic equilibrium. Let us introduce the perturbation fields

$$\mathbf{X} = (X_1, X_2, X_3, X_4)^{\mathrm{T}} \equiv (S - \bar{S},\, I - \bar{I},\, B - \bar{B},\, R - \bar{R}).$$

The system governing the evolution of the perturbation fields is

$$\dot{\mathbf{X}} = L\mathbf{X} + \mathbf{F} \tag{18}$$

with $\mathbf{F} = (F_1, -F_1, F_2, 0)^{\mathrm{T}}$ and

$$L = \begin{pmatrix} a_{11} & 0 & a_{13} & 0 \\ a_{21} & a_{22} & a_{23} & 0 \\ 0 & a_{32} & a_{33} & 0 \\ 0 & a_{42} & 0 & a_{44} \end{pmatrix}, \quad a_{11} = -\left(\frac{\beta\bar{B}}{K_B + \bar{B}} + \mu\right),$$

$$a_{13} = -\frac{\beta\bar{S}K_B}{(K_B + \bar{B})^2}, \quad a_{21} = \frac{\beta\bar{B}}{K_B + \bar{B}}, \quad a_{22} = -(\mu + \delta), \quad a_{23} = -a_{13},$$

$$a_{32} = \xi, \quad a_{33} = r\left[2\bar{B} - \frac{3\bar{B}^2}{k} + \frac{2b\bar{B}}{k} - b\right] - \tau, \quad a_{42} = \delta, \quad a_{44} = -\mu,$$

$$F_1 = \frac{\beta K_B(\theta X_1 + \bar{S})}{(K_B + \theta X_3 + \bar{B})^3} X_3^2, \quad F_2 = -r\frac{\bar{B} - b}{k} X_3^2 + rX_3^2\left(1 - \frac{X_3 + \bar{B}}{k}\right) - \frac{r\bar{B}}{k} X_3^2.$$

In order to perform the linear stability of the biologically meaningful equilibria, let us consider the linearized version of (18). The spectral equation of L is

$$(\lambda - a_{44})\left(\lambda^3 - \mathrm{I}_1\lambda^2 + \mathrm{I}_2\lambda - \mathrm{I}_3\right) = 0, \tag{19}$$

where I_j $(j = 1, 2, 3)$ are the principal invariants of

$$\tilde{L} = \begin{pmatrix} a_{11} & 0 & a_{13} \\ a_{21} & a_{22} & a_{23} \\ 0 & a_{32} & a_{33} \end{pmatrix}. \tag{20}$$

Equation (19) admits the root $\lambda = a_{44} < 0$ and the roots of the equation

$$\lambda^3 - \mathrm{I}_1\lambda^2 + \mathrm{I}_2\lambda - \mathrm{I}_3 = 0. \tag{21}$$

The null solution of linearized system is stable if and only if all the roots of (21) have negative real part. The necessary and sufficient conditions, guaranteeing that all the roots of (21) have negative real part, are the Routh–Hurwitz conditions [18]

$$\mathrm{I}_1 < 0, \qquad \mathrm{I}_3 < 0, \qquad \mathrm{I}_1\mathrm{I}_2 - \mathrm{I}_3 < 0, \tag{22}$$

which imply necessarily that $I_2 > 0$.

Remark 1. Let us remark that if $a_{33} > 0$, it follows that $\mathrm{I}_3 > 0$.

Let us start by investigating the linear stability of the disease-free equilibrium $(N_0, 0, 0, 0)$. When $\bar{S} = N_0$, $\bar{I} = \bar{B} = \bar{R} = 0$, invariants can be written as

$$\begin{aligned} &\mathrm{I}_1 = -2\mu - \delta - \tau - rb < 0, \qquad \mathrm{I}_3 = \mu(\mu+\delta)(\tau+rb)(\mathcal{R}_0 - 1), \\ &\mathrm{I}_2 = \mu(\mu+\delta+\tau+rb) + (\mu+\delta)(\tau+rb)(1-\mathcal{R}_0). \end{aligned} \tag{23}$$

The following theorem holds.

Theorem 3. *If $\mathcal{R}_0 < 1$, the disease-free equilibrium is linearly stable.*

Proof. In view of (23), it turns out that $\mathrm{I}_1 < 0$ and $\mathrm{I}_3 < 0 \Leftrightarrow \mathcal{R}_0 < 1$, $\mathrm{I}_2 > 0 \Leftrightarrow \mathcal{R}_0 < 1$. Furthermore, $\mathcal{R}_0 < 1$ yields

$$\begin{aligned} \mathrm{I}_1\mathrm{I}_2 - \mathrm{I}_3 = &-\mu(2\mu+\delta+\tau+rb)(\mu+\delta+\tau+rb) \\ &- (\mu+\delta)(\tau+rb)(\mu+\delta+\tau+rb)(1-\mathcal{R}_0) < 0. \end{aligned}$$

Going on to examine now the stability of the endemic equilibrium $\bar{E} = (\bar{S}, \bar{I}, \bar{B}, \bar{R})$, the principal invariants become

$$\begin{aligned} \mathrm{I}_1 &= \frac{r(-bk + 2(b+k)\bar{B} - 3\bar{B}^2)}{k} - \frac{\bar{B}\beta}{K_B + \bar{B}} - \delta - 2\mu - \tau, \\ \mathrm{I}_2 &= \left(\frac{\bar{B}\beta}{(K_B+\bar{B})} + \mu\right)(\delta+\mu) - \frac{K_B\bar{S}\beta\xi}{(K_B+\bar{B})^2} \\ &\quad + \frac{[K_B(\delta+2\mu) + \bar{B}(\beta+\delta+2\mu)][k\tau + br(k-2\bar{B}) - r(2k-3\bar{B})\bar{B}]}{k(K_B+\bar{B})}, \\ \mathrm{I}_3 &= \frac{1}{k(K_B+\bar{B})^2}\big[kK_B\bar{S}\beta\mu\xi - (K_B+\bar{B})(\delta+\mu)\big(K_B\mu + \bar{B}(\beta+\mu)\big) \\ &\quad \times \big(br(k-2\bar{B}) + r\bar{B}(-2k+3\bar{B}) + k\tau\big)\big]. \end{aligned}$$

Finding necessary and sufficient conditions guaranteeing that (22) are verified is quite complicated due to the presence of a lot of parameters. Sufficient conditions ensuring linear stability of the endemic equilibrium have been found, but we prefer not to report them so as not to weigh down the paper. □

5 Bifurcation analysis

5.1 Backward bifurcation

In general, it is observed that disease will eradicate (i.e. the disease free equilibrium will be stable) when $\mathcal{R}_0 < 1$, while disease persists when $\mathcal{R}_0 > 1$. The analysis of some epidemic models depicts that a stable endemic equilibrium exists even when $\mathcal{R}_0 < 1$. This phenomenon is known as backward bifurcation. In other words, a backward bifurcation at $\mathcal{R}_0 = 1$ may qualitatively be described as follows. In the neighboring of 1, for

$\mathcal{R}_0 < 1$, an equilibrium corresponding to a smaller number of infective individuals, which is unstable, appears, while the disease-free equilibrium and an equilibrium corresponding to a larger number of infective individuals are locally asymptotically stable. Epidemiologically, a backward bifurcation means that it is not enough to simply reduce the basic reproductive number to a value less than one to eradicate a disease. The occurrence of either a forward or a backward bifurcation can have important consequences from the point of view of the disease control and thus for the eradication of the disease. In order to investigate the possibility of backward bifurcation, we choose β as bifurcation parameter, and we obtain the value β^* of β at $\mathcal{R}_0 = 1$ given by $\beta^* = K_B(\mu+\delta)(\tau+rb)/(N_0\xi)$. The Jacobian of (1)–(4) evaluated in E_0 at $\beta = \beta^*$ is given by

$$J_{\beta^*}^{E_0} = \begin{pmatrix} -\mu & 0 & \frac{-\beta^* N_0}{K_B} \\ 0 & -(\mu+\delta) & \frac{\beta^* N_0}{K_B} \\ 0 & \xi & -(rb+\tau) \end{pmatrix}.$$

The eigenvalues of $J_{\beta^*}^{E_0}$ are

$$\psi_1 = -\mu, \qquad \psi_2 = -2(\mu+\delta+rb+\tau), \qquad \psi_3 = 0.$$

Since $\psi_3 = 0$ is a simple zero eigenvalue of $J_{\beta^*}^{E_0}$, then the disease free equilibrium E_0 is non hyperbolic equilibrium. Hence, the model at the hand is an eligible candidate to apply the center manifold theory [8]. Let us denote by $\mathbf{w} = (w_1, w_2, w_3)^{\mathrm{T}}$ a right eigenvector corresponding to the zero eigenvalue $\psi_3 = 0$. It follows

$$-\mu w_1 - \frac{\beta^* N_0}{K_B} w_3 = 0, \qquad -(\mu+\delta)w_2 + \frac{\beta^* N_0}{K_B} w_3 = 0,$$
$$\xi w_2 - (rb+\tau)w_3 = 0,$$

which gives

$$\mathbf{w} = \left(\frac{-(rb+\tau)(\mu+\delta)}{\xi\mu}, \frac{(rb+\tau)}{\xi}, 1 \right)^{\mathrm{T}}.$$

Furthermore, the left eigenvector $\theta = (\theta_1, \theta_2, \theta_3)$ satisfying $w \cdot \theta = 1$ is given by

$$-\mu\theta_1 = 0, \qquad -(\mu+\delta)\theta_2 + \xi\theta_3 = 0,$$
$$-\frac{\beta^* N_0}{K_B}\theta_1 + \frac{\beta^* N_0}{K_B}\theta_2 - (rb+\tau)\theta_3 = 0.$$

The left eigenvector is

$$\theta = \left(0, \frac{\xi}{\mu+\delta+rb+\tau}, \frac{\mu+\delta}{\mu+\delta+rb+\tau} \right).$$

We can thus compute the coefficients from Theorem 4.1 given in [8] as follows:

$$\bar{a} = \sum_{h,i,j=1}^{3} \theta_h w_i w_j \frac{\partial^2 f_h}{\partial x_i \partial x_j}(E_0, \beta^*), \qquad \bar{b} = \sum_{h,i=1}^{3} \theta_h w_i \frac{\partial^2 f_h}{\partial x_i \partial \beta}(E_0, \beta^*).$$

Considering in $\bar{a}$ and $\bar{b}$ only the nonzero terms, it follows that

$$\bar{a} = 2\theta_2 w_1 w_3 \frac{\partial^2 f_2}{\partial S \partial B}(E_0, \beta^*) + \theta_2 w_3^2 \frac{\partial^2 f_2}{\partial B^2}(E_0, \beta^*) + \theta_3 w_3^2 \frac{\partial^2 f_3}{\partial B^2}(E_0, \beta^*)$$

and

$$\bar{b} = \theta_2 w_3 \frac{\partial^2 f_2}{\partial B \partial \beta}(E_0, \beta^*).$$

Using the values of left and right eigenvectors, we get

$$\bar{a} = \frac{2}{(rb + \tau + \mu + \delta)} \left[(\mu + \delta) \left(\frac{\beta(rb + \tau)}{K_B \mu} + \frac{r(b + k)}{k} \right) - \frac{\xi \beta N_0}{K_B^3} \right],$$
$$\bar{b} = \frac{\xi N_0}{K_b(rb + \tau + \mu + \delta)}.$$

Observe that the coefficient $\bar{b}$ is always positive and $\bar{a} > 0$ when

$$(\mu + \delta) \left[\frac{\beta(rb + \tau)}{K_B \mu} + \frac{r(b + k)}{k} \right] > \frac{\xi \beta N_0}{K_B^3}.$$

If we set $\mathcal{R}^* = (\mu + \delta) K_B^3 / (\xi \beta N_0)[\beta(rb+\tau)/(K_B \mu) + r(b+k)/k]$, using Theorem 4.1 in [8], we can state the following theorem.

Theorem 4. *If $\mathcal{R}^* > 1$, system* (1)–(4) *exhibits a backward bifurcation when $\mathcal{R}_0 = 1$. If $\mathcal{R}^* < 1$, system* (1)–(4) *exhibits a forward bifurcation when $\mathcal{R}_0 = 1$.*

5.2 Investigation on the onset of Hopf bifurcation

Hopf bifurcation is represented as the appearance or disappearance of a periodic orbit through a local change in the stability properties of an equilibrium point. In this section, we explore the possibility of occurrence of Hopf bifurcation and the direction of Hopf bifurcation around the interior equilibrium point $\bar{E}$ with respect to the bifurcating parameter ξ. If

$$\begin{aligned} &\mathrm{I}_1 < 0, \\ &\mathrm{I}_3 < 0, \\ &\mathrm{I}_1 \mathrm{I}_2 - \mathrm{I}_3 = 0, \end{aligned} \tag{24}$$

in correspondence of an interior equilibrium, Eq. (21) gives the following eigenvalues:

$$\lambda_{1,2} = \pm \mathrm{i}\omega_0, \quad \lambda_3 = \mathrm{I}_1 \quad \text{with } \omega_0 = \sqrt{\frac{\mathrm{I}_3}{\mathrm{I}_1}}. \tag{25}$$

In view of Remark 1, let $a_{33} < 0$ and ξ^* be the critical value of the Hopf bifurcation parameter given by

$$\xi^* = \frac{(a_{11} + a_{22})(a_{11} + a_{33})(a_{22} + a_{33})}{a_{23}(a_{22} + a_{33} - a_{21})} > 0.$$

When (24) holds, in order to investigate the existence of Hopf bifurcation, we first need to check the transversality condition, which confirms that the eigenvalues cross the imaginary axis of the complex plane with non zero speed, i.e. $\mathrm{d}\mathrm{Re}(\lambda)/\mathrm{d}\xi|_{\xi=\xi^*} \neq 0$. When the value of the parameter ξ changes around the Hopf bifurcation point, the two imaginary eigenvalues $\pm \mathrm{i}\omega_0$ will become complex eigenvalues written as $\lambda = v(\xi) \pm \mathrm{i}\omega(\xi)$. Substituting $\lambda = v + \mathrm{i}\omega$ into (21) and separating the real and imaginary parts, we obtain

$$v^3 + (\mathrm{I}_1 - 3v)\omega^2 - \mathrm{I}_1 v^2 + \mathrm{I}_2 v - \mathrm{I}_3 = 0, \tag{26}$$

$$-\omega^3 + 3v^2\omega - 2\mathrm{I}_1 v\omega + \mathrm{I}_2\omega = 0. \tag{27}$$

From (27) we find ω, and replacing in (26), we obtain, with $f(v) = 3v^2 - 2\mathrm{I}_1 v + \mathrm{I}_2$,

$$v^3 - \mathrm{I}_1 v^2 + \big(\mathrm{I}_2 - 3f(v)\big)v + \big(f(v)\big)\mathrm{I}_1 - \mathrm{I}_3\big) = 0. \tag{28}$$

Differentiating v with respect to ξ and evaluating for $\xi = \xi^*$, we get

$$\left.\frac{\mathrm{d}v}{\mathrm{d}\xi}\right|_{\xi=\xi^*} = \frac{-K_B\bar{S}\beta\mu}{(\bar{B}+K_B)^2(-2\mathrm{I}_2|_{\xi=\xi^*} - \mathrm{I}_1|_{\xi=\xi^*})}, \tag{29}$$

so the transversality condition for Hopf bifurcation is satisfied. Thus, it appears that a Hopf bifurcation around the interior equilibrium occurs at $\xi = \xi^*$.

The above results can be summarized in the following theorem.

Theorem 5. *For model* (1)–(4)*, if* $a_{33} < 0$ *and* $I_3 < 0$*, then there exists a Hopf bifurcation emerging from its positive interior equilibrium when the contribution of each infected person to the population of bacteria,* ξ*, passes through the critical value* ξ^**.*

We have obtained some conditions under which system (1)–(4) undergoes Hopf bifurcation from an interior equilibrium at $\xi = \xi^*$. Now, we discuss the direction of Hopf bifurcation and the stability of the bifurcating periodic solution. The method used is based on the normal form theory and the center manifold reduction.

Denoting by $\bar{\mathbf{X}} \equiv (X_1, X_2, X_3)^{\mathrm{T}}$, expansion of Taylor's series up to terms of order 3 (by neglecting the higher-order terms of degree 4 and above), omitting the bar, produces the following system:

$$\dot{\mathbf{X}} = \tilde{L}\mathbf{X} + \tilde{A}(\mathbf{X}), \tag{30}$$

where $\tilde{L}$ is given by (20), and

$$\tilde{A}(\mathbf{X}) = \begin{pmatrix} \frac{\beta K_B\bar{S}}{(K_B+\bar{B})^3}X_3^2 - \frac{\beta K_B}{(K_B+\bar{B})^2}X_1X_3 - \frac{\beta K_B\bar{S}}{(K_B+\bar{B})^4}X_3^3 + \frac{\beta K_B}{(K_B+\bar{B})^3}X_1X_3^2 + O(4) \\ -\frac{\beta K_B\bar{S}}{(K_B+\bar{B})^3}X_3^2 + \frac{\beta K_B}{(K_B+\bar{B})^2}X_1X_3 + \frac{\beta K_B\bar{S}}{(K_B+\bar{B})^4}X_3^3 - \frac{\beta K_B}{(K_B+\bar{B})^3}X_1X_3^2 + O(4) \\ [r(1-\frac{\bar{B}}{k}) - \frac{r}{k}(2\bar{B}-b)]X_3^2 - \frac{r}{k}X_3^3 + O(4) \end{pmatrix}.$$

Let $\mathbf{X} = P\mathbf{Y}$, where $\mathbf{Y} = (Y_1, Y_2, Y_3)^{\mathrm{T}}$ and

$$P = \begin{pmatrix} p_{11} & 0 & p_{13} \\ p_{21} & p_{22} & p_{23} \\ p_{31} & p_{32} & p_{33} \end{pmatrix}$$

with

$$\begin{aligned}
&p_{11} = -a_{13}, && p_{12} = 0, && p_{13} = -a_{13},\\
&p_{21} = \frac{-a_{33}a_{11} + \omega_0^2}{\xi^*}, && p_{22} = \frac{(a_{33}+a_{11})\omega_0}{\xi^*}, && p_{23} = \frac{-(a_{33}a_{11}+a_{22}I_1)}{\xi^*},\\
&p_{31} = a_{11}, && p_{32} = -\omega_0, && p_{33} = -(a_{22} + a_{33}).
\end{aligned} \tag{31}$$

Under this transformation, system (30) becomes

$$\dot{\mathbf{Y}} = (P^{-1}\tilde{L}P)\mathbf{Y} + P^{-1}\tilde{A}(P\mathbf{Y}), \tag{32}$$

where P^{-1} denotes the inverse

$$P^{-1} = \begin{pmatrix} p_{11}^{(-1)} & p_{12}^{(-1)} & p_{13}^{(-1)} \\ p_{21}^{(-1)} & p_{22}^{(-1)} & p_{23}^{(-1)} \\ p_{31}^{(-1)} & p_{32}^{(-1)} & p_{33}^{(-1)} \end{pmatrix}$$

with

$$\begin{aligned}
&p_{11}^{(-1)} = \frac{p_{22}p_{33} - p_{23}p_{32}}{\det P}, && p_{12}^{(-1)} = \frac{p_{13}p_{32}}{\det P}, && p_{13}^{(-1)} = \frac{p_{22}p_{13}}{\det P},\\
&p_{21}^{(-1)} = \frac{-(p_{21}p_{33}-p_{31}p_{23})}{\det P}, && p_{22}^{(-1)} = \frac{p_{11}p_{33}-p_{13}p_{31}}{\det P}, && p_{23}^{(-1)} = \frac{p_{11}p_{23}-p_{21}p_{13}}{\det P},\\
&p_{31}^{(-1)} = \frac{(p_{21}p_{32}-p_{31}p_{22})}{\det P}, && p_{32}^{(-1)} = -\frac{p_{11}p_{32}}{\det P}, && p_{33}^{(-1)} = \frac{p_{11}p_{22}}{\det P}.
\end{aligned}$$

Then system (32) can be written as

$$\begin{pmatrix} \dot{Y}_1 \\ \dot{Y}_2 \\ \dot{Y}_3 \end{pmatrix} = \begin{pmatrix} 0 & \omega_0 & 0 \\ -\omega_0 & 0 & 0 \\ 0 & 0 & \mathrm{I}_1 \end{pmatrix} \begin{pmatrix} Y_1 \\ Y_2 \\ Y_3 \end{pmatrix} + \begin{pmatrix} \tilde{f}_1^{(-1)} \\ \tilde{f}_2^{(-1)} \\ \tilde{f}_3^{(-1)} \end{pmatrix}, \tag{33}$$

where

$$\begin{aligned}
\tilde{f}_1^{(-1)} = {} & (p_{31}Y_1 + p_{32}Y_2 + p_{33}Y_3)\Big\{\frac{1}{k}\Big[p_{13}^{(-1)}r(b - 3\bar{B} + k - p_{31}Y_1 - p_{32}Y_2 - p_{33}Y_3)\\
& \times (p_{31}Y_1 + p_{32}Y_2 + p_{33}Y_3)\Big] - \frac{\beta}{(\bar{B}+K_B)^4}K_B(p_{11}^{(-1)} - p_{12}^{(-1)})(\bar{B} + K_B\\
& - p_{31}Y_1 - p_{32}Y_2 - p_{33}Y_3)\big[p_{11}K_BY_1 + p_{13}K_BY_3 + \bar{B}(p_{11}Y_1 + p_{13}Y_3)\\
& - \bar{S}(p_{31}Y_1 + p_{32}Y_2 + p_{33}Y_3)\big]\Big\},\\
\tilde{f}_2^{(-1)} = {} & (p_{31}Y_1 + p_{32}Y_2 + p_{33}Y_3)\Big\{\frac{1}{k}\Big[p_{23}^{(-1)}r(b - 3\bar{B} + k - p_{31}Y_1 - p_{32}Y_2 - p_{33}Y_3)\\
& \times (p_{31}Y_1 + p_{32}Y_2 + p_{33}Y_3)\Big] - \frac{\beta}{(\bar{B}+K_B)^4}K_B(p_{21}^{(-1)} - p_{22}^{(-1)})(\bar{B} + K_B
\end{aligned}$$

$$
\begin{aligned}
&- p_{31}Y_1 - p_{32}Y_2 - p_{33}Y_3\big)\big[p_{11}K_BY_1 + p_{13}K_BY_3 + \bar{B}(p_{11}Y_1 + p_{13}Y_3)\\
&- \bar{S}(p_{31}Y_1 + p_{32}Y_2 + p_{33}Y_3)\big]\Bigg\},\\
\tilde{f}_3^{(-1)} &= (p_{31}Y_1 + p_{32}Y_2 + p_{33}Y_3)\Bigg\{\frac{1}{k}\Big[p_{33}^{(-1)}r(b - 3\bar{B} + k - p_{31}Y_1 - p_{32}Y_2 - p_{33}Y_3)\\
&\times (p_{31}Y_1 + p_{32}Y_2 + p_{33}Y_3)\Big] - \frac{\beta}{(\bar{B} + K_B)^4}K_B(p_{31}^{(-1)} - p_{32}^{(-1)})(\bar{B} + K_B\\
&- p_{31}Y_1 - p_{32}Y_2 - p_{33}Y_3\big)\big[p_{11}K_BY_1 + p_{13}K_BY_3 + \bar{B}(p_{11}Y_1 + p_{13}Y_3)\\
&- \bar{S}(p_{31}Y_1 + p_{32}Y_2 + p_{33}Y_3)\big]\Bigg\}.
\end{aligned}
$$

There exists a center manifold for (33), which can be represented as

$$W^C(0) = \big\{(Y_1, Y_2, Y_3) \in \mathbb{R}^3\colon\ Y_3 = h^*(Y_1, Y_2),\ h^*(0,0) = 0,\ Dh^*(0,0) = 0\big\}.$$

We assume $h^*(Y_1, Y_2) = b_1Y_1^2 + b_2Y_2^2 + b_3Y_1Y_2 + \cdots$. Through approximate computation for the center manifold, we obtain

$$
\begin{aligned}
b_1 &= -b_2 + \frac{1}{I_1}\big[\big(p_{32}^{(-1)} - p_{31}^{(-1)}\big)\big(f_{11}^{(1)} + f_{22}^{(1)}\big) - p_{33}^{(-1)}\big(f_{11}^{(3)} + f_{22}^{(3)}\big)\big],\\
b_2 &= \frac{1}{4\omega_0^2 + I_1^2}\Bigg\{\big[\big(p_{32}^{(-1)} - p_{31}^{(-1)}\big)f_{22}^{(1)} - p_{33}^{(-1)}f_{22}^{(3)}\big]\left(I_1 + \frac{2\omega_0^2}{I_1}\right)\\
&\quad + \big(p_{32}^{(-1)} - p_{31}^{(-1)}\big)\left(\frac{2\omega_0^2}{I_1}f_{11}^{(1)} + \omega_0 f_{12}^{(1)}\right) - p_{33}^{(-1)}\left(\frac{2\omega_0^2}{I_1}f_{11}^{(3)} + \omega_0 f_{12}^{(3)}\right)\Bigg\},\\
b_3 &= \frac{1}{\omega_0}\big[I_1b_2 + \big(p_{31}^{(-1)} - p_{32}^{(-1)}\big)f_{22}^{(1)} + p_{33}^{(-1)}f_{22}^{(3)}\big],
\end{aligned}
$$

where

$$
\begin{aligned}
f_{11}^{(1)} &= \frac{\beta K_B\bar{S}}{(K_B+\bar{B})^3}a_{11}^2 + \frac{\beta K_B}{(K_B+\bar{B})^2}a_{11}a_{13}, & f_{22}^{(1)} &= \frac{\beta K_B\bar{S}}{(K_B+\bar{B})^3}\omega_0^2,\\
f_{11}^{(3)} &= \left(r\left(1-\frac{\bar{B}}{k}\right) - \frac{r}{k}(2\bar{B}-b)\right)a_{11}^2, & f_{22}^{(3)} &= \left(r\left(1-\frac{\bar{B}}{k}\right) - \frac{r}{k}(2\bar{B}-b)\right)\omega_0^2,\\
f_{12}^{(1)} &= 2\frac{\beta K_B\bar{S}}{(K_B+\bar{B})^3}a_{11}\omega_0 + \frac{\beta K_B}{(k_B+\bar{B})^2}a_{13}\omega_0, & f_{12}^{(3)} &= -2a_{11}\omega_0\left(r\left(1-\frac{\bar{B}}{k}\right) - \frac{r}{k}(2\bar{B}-b)\right).
\end{aligned}
$$

System (33) restricted to the center manifold is given by

$$\begin{pmatrix}\dot{Y}_1\\ \dot{Y}_2\end{pmatrix} = \begin{pmatrix}0 & \omega_0\\ -\omega_0 & 0\end{pmatrix}\begin{pmatrix}Y_1\\ Y_2\end{pmatrix} + \begin{pmatrix}\tilde{f}^1(Y_1, Y_2)\\ \tilde{f}^2(Y_1, Y_2)\end{pmatrix}, \tag{34}$$

where

$$
\begin{aligned}
\tilde{f}^1(Y_1, Y_2) &= \tilde{f}_1^{(-1)}\big(Y_1, Y_2, h^*(Y_1, Y_2)\big),\\
\tilde{f}^2(Y_1, Y_2) &= \tilde{f}_2^{(-1)}\big(Y_1, Y_2, h^*(Y_1, Y_2)\big).
\end{aligned}
$$

The 1st Lyapunov coefficient based on the normal form (34), which determines the stability and direction of periodic solution, is given by

$$l_1 = \frac{1}{16}\big[\tilde{f}^1_{Y_1Y_1Y_1} + \tilde{f}^1_{Y_1Y_2Y_2} + \tilde{f}^2_{Y_1Y_1Y_2} + \tilde{f}^2_{Y_2Y_2Y_2}\big] + \frac{1}{16\omega_0}\big[\tilde{f}^1_{Y_1Y_2}\big(f^1_{Y_1Y_1} + f^1_{Y_2Y_2}\big) - \tilde{f}^2_{Y_1Y_2}\big(f^2_{Y_1Y_1} + f^2_{Y_2Y_2}\big) - \tilde{f}^1_{Y_1Y_1}\tilde{f}^2_{Y_1Y_1} + \tilde{f}^1_{Y_2Y_2}\tilde{f}^2_{Y_2Y_2}\big], \tag{35}$$

where all the derivatives are calculated at the bifurcation point $(Y_1, Y_2, \xi) = (0, 0, \xi^*)$. Then Hopf bifurcation is supercritical if $l_1 < 0$ or subcritical if $l_1 > 0$.

6 Sensitivity analysis

To understand the importance of parameters, which are responsible for the transmission of a disease, we perform a sensitivity analysis. It tells which parameters deserve the most numerical attention: a highly sensitive parameter should be carefully estimated as a small variation in it may lead to large changes in the quantity of interest and qualitatively different results. An insensitive parameter does not require as much effort to be estimated. The initial disease transmission is directly related to $\mathcal{R}_0$; for this reason, we calculate the sensitivity indices of the basic reproductive number $\mathcal{R}_0$. Let p a generic parameter of model (1)–(4). The normalized forward sensitivity index of $\mathcal{R}_0$ (which is differentiable with respect to p) is defined as

$$\Pi^{\mathcal{R}_0}_p = \frac{p}{\mathcal{R}_0}\frac{\partial \mathcal{R}_0}{\partial p}. \tag{36}$$

If this index is negative (positive), then the relationship between the parameter and $\mathcal{R}_0$ is of inverse (direct) proportion. The index modulus is an indicator of the size of the effect of changes in that parameter. As we have an explicit expression of $\mathcal{R}_0$, we derive an analytical expression for the sensitivity of $\mathcal{R}_0$ to each of the different parameters of model (1)–(4). Precisely,

$$\begin{aligned} &\Pi^{\mathcal{R}_0}_\beta = \Pi^{\mathcal{R}_0}_\xi = -\Pi^{\mathcal{R}_0}_{K_B} = 1, \qquad \Pi^{\mathcal{R}_0}_r = \Pi^{\mathcal{R}_0}_b = -\frac{rb}{rb+\tau}, \\ &\Pi^{\mathcal{R}_0}_\mu = -\frac{\mu}{\mu+\delta}, \qquad \Pi^{\mathcal{R}_0}_\delta = -\frac{\delta}{\mu+\delta}, \qquad \Pi^{\mathcal{R}_0}_\tau = -\frac{\tau}{\tau+rb}. \end{aligned} \tag{37}$$

From (37) we can see that the sensitivity indices of $\mathcal{R}_0$ with respect to β, ξ, K_B do not depend on any parameter values, while the other indices have an obvious structure depending on some parameters. From an initial analysis, $\mathcal{R}_0$ is most sensitive to the contact rate with contaminated water (β) and to the contribution of each infected person to the population of bacteria (ξ) (as shown in (37)). This result shows that any increase (decrease) by a given percentage in β or ξ will increase (decrease) by the same percentage the value of $\mathcal{R}_0$. The other parameter with highest sensitivity index is K_B with $\Pi^{\mathcal{R}_0}_{K_B} = -1$. Increasing (decreasing) K_B by a given percentage will decrease (increase) $\mathcal{R}_0$ by the same percentage. The other parameters have a minor effect on $\mathcal{R}_0$. In fact, from (37) the analytical expression for the sensitivity of $\mathcal{R}_0$ to any of the other parameters, evaluated

Table 2. Baseline values of model parameters and sensitivity indices of $\mathcal{R}_0$ to such parameters evaluated at the baseline parameter values.

	β	ξ	K_B	r	b	δ	μ	τ
Baseline values	1	10	10000	0.5	10	0.25	0.02	0.15
Sensitivity index	+1	+1	−1	−0.97	−0.97	−0.92	−0.07	−0.03

Table 3. Parameters values for the two examples.

	N_0	μ	δ	ξ	K_B	τ	r	β	b	k
Example 1	1000	0.02	0.25	10	10000	0.15	0.50	1	10	100
Example 2	10000	0.02	0.25	10	10000	0.15	0.25	2.5	300	500

in absolute value, is less than 1. For all parameters, the sign of the sensitivity indices of $\mathcal{R}_0$ agrees with an intuitive expectation. In order to effectively measure, the relative change in $\mathcal{R}_0$ when the remaining parameters change, one has to evaluate the sensitivity indices at the chosen baseline parameter values. However, following the procedure used by [9], we can replace τ and r (keeping b fixed) by the parameters $\zeta = rb + \tau$, $\hat{\theta} = r/\tau$, where ζ can be seen as the linear loss rate of bacteria. Measuring the sensitivity of $\mathcal{R}_0$ with respect to ζ, keeping $\hat{\theta}$ fixed (allowing r and τ to vary, while their ratio remains fixed), it follows that $\Pi_{\zeta}^{\mathcal{R}_0} = \Pi_{r}^{\mathcal{R}_0} + \Pi_{\tau}^{\mathcal{R}_0} = -1$ so providing a good estimate of the joint impact of r and τ. This means that the aggregate parameter ζ is one of the most sensitive parameters. (Similarly, one can proceed replacing τ and b, keeping r fixed, with $\Gamma = rb + \tau$ and $\bar{\theta} = b/\tau$, respectively, and obtain $\Pi_{\Gamma}^{\mathcal{R}_0} = \Pi_{b}^{\mathcal{R}_0} + \Pi_{\tau}^{\mathcal{R}_0} = -1$.) With a similar procedure, one can estimate the joint effect of δ and μ by the sensitivity index of $\mathcal{R}_0$ with respect to $\eta = \delta + \mu$, i.e. $\Pi_{\eta}^{\mathcal{R}_0} = \Pi_{\delta}^{\mathcal{R}_0} + \Pi_{\mu}^{\mathcal{R}_0} = -1$. The parameter $\mu + \delta$ can be seen as the total loss rate of infective individuals. In Table 2, the values of all the parameters displayed in the first line are taken as the baseline values and are the same of Example 1 in Table 3. They are used to evaluate, through (36), the sensitivity indices of the remaining parameters, which are responsible for the transmission and management of a waterborne disease, in relation to the basic reproduction number $\mathcal{R}_0$. The results of such calculation are presented in the second line of Table 2. The parameters are ordered from the most sensitive to the least.

7 Numerical simulations and discussion

In this section, we investigate by numerical simulations some different scenarios for the proposed model and discuss the obtained results. Throughout these experiments, we also intend to highlight the impact of the assumption of a nonlinear pathogen growth on the infected dynamics: by tuning the parameter r governing this growth, we will show the higher flexibility of the present model in reproducing different epidemic outbreaks.

7.1 Disease dynamics and basic reproduction number

Specifically, we explore two situations: in the first example, we set the model parameters to obtain a basic reproduction number $\mathcal{R}_0$ less than one so that the disease-free equilib-

rium is stable; in the second example, we choose the parameters to obtain $\mathcal{R}_0$ greater than one and to have two endemic equilibria in the interval $(0, b_1)$. All the parameters values for the two examples are reported in Table 3. In the exploratory study [10], a model has been introduced to capture Cholera transmission within a community. This model has been a predecessor of several more recent ones. As discussed in [13], true values of the parameters in all these models are often difficult or impossible to estimate accurately. That work also reports the most common setting of several key parameter values across the main published models. So we choose accordingly the parameter values for the numerical experiments. Such simulations have the only purpose of showing the ability of the proposed model to represent different scenarios for the waterborne disease evolution. Of course, running such simple models against real data (as we did in a different model setting in [7]) could just reproduce the initial outbreak of an epidemy before the planning and execution of human interventions, like vaccination or water sanitation, that are not yet represented in the current formulation. More realistic models, including terms representing such interventions, could be considered in future work and undoubtedly could benefit from these preliminary studies.

Example 1. We get $\mathcal{R}_0 \approx 0.72$, $b_1 \approx 10.334$, $k_1 \approx 99.667$, and the polynomial $T(B)$ introduced in Section 4 has two positive roots, one in the interval $(0, b_1)$, the so-called lower branch, and one greater than k_1 (upper branch). These roots correspond to two endemic equilibria with approximate values of the variables S, I, B given by $E_1 \approx (986, 1, 2.795)$, $E_{\text{up}} \approx (659, 25, 104.777)$, while for the disease-free equilibrium, we find $E_0 = (1000, 0, 0)$. Now, according to the linear stability analysis, E_0 and E_{up} are stable equilibria, but E_1 is unstable. The left panel of Fig. 1 shows trajectories for $S(t)$, $I(t)$ and $B(t)$ starting from the initial point $(900, 0, 5)$ and reaching the disease-free equilibrium (left panel). In the same parameters setting, different initial conditions with $I(0) > 0$ lead to the endemic equilibrium E_{up}. This can be clearly seen in the right panel of the same Fig. 1.

When $\mathcal{R}_0$ is greater than one, the polynomial $T(B)/B$, along with the always existent root greater than k_1, can have either zero or two positive roots. We decided to consider this

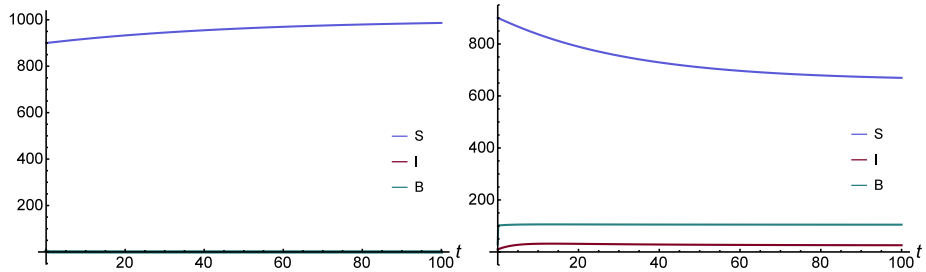

Figure 1. In the left panel, the trajectories of $S(t)$ (blue line), $I(t)$ (red line), $B(t)$ (green line) are shown in the parameter setting of Example 1 with $S(0) = 900$, $I(0) = 0$ and $B(0) = 5$; the trajectories reach the disease-free equilibrium $E_0 = (1000, 0, 0)$. In the right panel, it is $I(0) = 10$, $B(0) = 30$, and the trajectories reach the endemic equilibrium $E_{\text{up}} \approx (659, 25, 105)$. Note that the variable $R(t)$ is not plotted since it is completely determined by S, I and N_0.

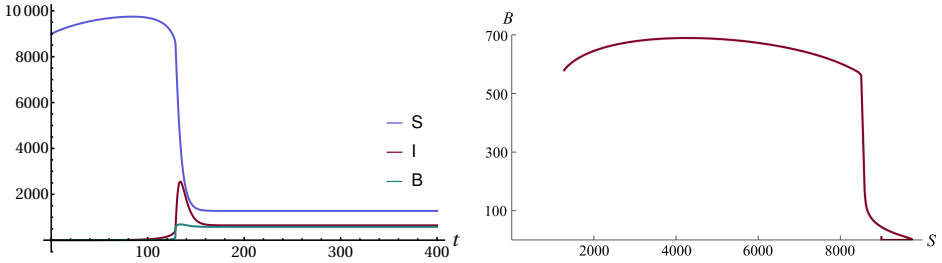

Figure 2. In the left panel, a plot showing the trajectories of $S(t)$ (blue line), $I(t)$ (red line), $B(t)$ (green line) in the parameter setting of Example 2 with initial conditions $S(0) = 9000$, $I(0) = 0$, $B(0) = 10$. In this setting, the trajectories reach the endemic equilibrium $E_{\rm up} \approx (1275, 646, 579)$. In the right panel, a phase-plane plot of $S(t)$ and $B(t)$ is shown.

latter situation to further investigate these endemic equilibria. Then we present a second example.

Example 2. For the parameter setting reported in the second row of Table 3, we get $\mathcal{R}_0 \approx 1.23$, $b_1 \approx 302$, $k_1 \approx 498$, and the polynomial $T(B)$ introduced in Section 4 has three positive roots, two in the interval $(0, b_1)$ and one greater than k_1. These roots correspond to the three endemic equilibria E_1, E_2 and $E_{\rm up}$ with approximate values of the variables S, I, B given by $E_1 \approx (5918, 302, 55)$, $E_2 \approx (4835, 383, 86)$, $E_{\rm up} \approx (1275, 646, 579)$, while for the disease-free equilibrium, we find $E_0 = (10000, 0, 0)$. Now, according to the linear stability analysis, E_0, E_1 and E_2 are all unstable equilibria, while $E_{\rm up}$ is stable. Figure 2 reports the trajectories of $S(t)$ (blue line), $I(t)$ (red line) and $B(t)$ (green line) in this parameter setting. Starting from the initial conditions $S(0) = 9000$, $I(0) = 0$, $B(0) = 10$, the trajectories reach the endemic equilibrium $E_{\rm up} \approx (1275, 646, 579)$. In the right panel of the same figure, a phase-plane plot of $S(t)$ and $B(t)$ is shown.

7.2 Bifurcation scenarios

Now we intend to illustrate through numerical experiments some of the findings of Section 5. First, let us examine in both the reported examples how the chosen parameters (and the resulting value of the reproduction number $\mathcal{R}_0$) affect the stability of the endemic equilibria. The bifurcation diagrams in the left and right panels of Fig. 3 refer to Examples 1 and 2, respectively; in both cases, we vary the value of the contact rate β in the range $[1, 3]$ and report on the horizontal axis the resulting value of $\mathcal{R}_0$. It should be noted that in both panels, the upper branch equilibrium $B_{\rm up}$ (that always exists as previously shown) is stable and its value increases along with the value of $\mathcal{R}_0$. Moreover, the left panel shows how a unique lower branch equilibrium B_1 only exists for $\mathcal{R}_0 < 1$ (and it is always unstable). At $\mathcal{R}_0 = 1$, this equilibrium crosses the DFE, and a backward bifurcation occurs. The right panel reports a more interesting situation: while for $\mathcal{R}_0 < 1$, a single and unstable lower branch equilibrium exists, at $R_0 = 1$, a second equilibrium emerges (forward bifurcation), that is stable until $\mathcal{R}_0 = 1.0714$ and then becomes unstable. At $\mathcal{R}_0 = 1.2508$, both these equilibria disappear. Thus, for values of $\mathcal{R}_0$ higher than 1.0714, all trajectories converge to the upper branch equilibrium. To conclude, let us also

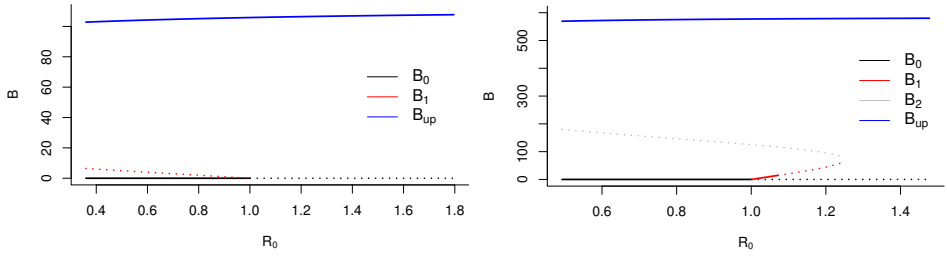

Figure 3. In the left panel, the B component of the system equilibria in the parameter setting of Example 1 plotted as functions of $\mathcal{R}_0$: the DFE B_0 (black line), the lower branch equilibrium B_1 (red line) and the upper branch equilibrium $B_{\rm up}$ (blue line). In all curves, a solid line represents a stable equilibrium, and a dotted line an unstable one. In the right panel, a similar plot for the parameter setting of Example 2. In this case, two lower branch equilibria exist, B_1 (red line) and B_2 (gray line).

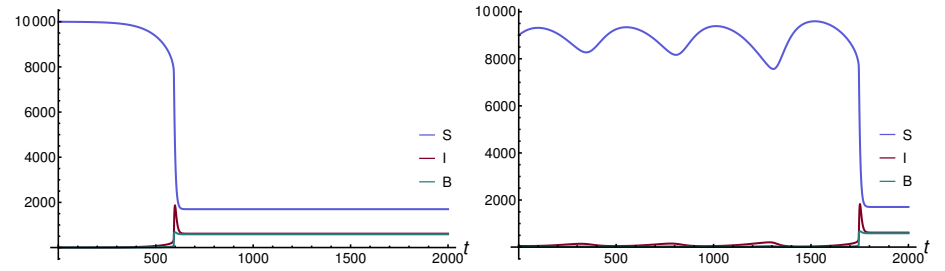

Figure 4. Left panel: trajectories for the S, I, B populations in the parameter setting of Example 2 in Table 3, apart from $\beta = 1.76$, $\xi = 12.0203$. With these choice, $E_1 \approx (8916, 80, 14)$ should show a Hopf bifurcation. However, the trajectories go towards the stable endemic equilibrium $E_{\rm up} \approx (1704, 615, 587)$. In the right panel, with slightly different parameter values ($\beta = 1.757$, $\xi = 12.03$) corresponding to linear stability of E_1, wide oscillations in the trajectories result in convergence to the other stable equilibrium $E_{\rm up}$.

present some numerical experiments concerning Hopf bifurcation. The analysis reported in Section 5.2 has proved how all the requirements can be met for the onset of a Hopf bifurcation on the endemic equilibrium $E_1 = (S_1.I_1, B_1)$ with $B_1 < b_1$. However, numerical experiments can hardly produce plots illustrating such a situation. This is due to the concurrent presence of a stable equilibrium $E_{\rm up}$ with $B_{\rm up} > k$ that eventually attracts the trajectories of the process. Then the best we can show is the extremely oscillating behaviour of the system trajectories when the parameter values are very close to the ones determining Hopf bifurcation. In the following, we will present some simulations to better clarify our findings. Let us fix all the parameter values as in Example 2 from Table 3, apart from β and ξ. Then we impose for ξ the critical value ξ^* defined in Section 5 and solve for (β, B) both (11) and $\mathrm{I}_3 < 0$. With these choices, we find $\beta = 1.76$, $\xi = 12.0203$, and the system admits three equilibrium points corresponding to the values $B_1 = 14.1534$, $B_2 = 86.7116$ and $B_{\rm up} = 586.775$ that are, respectively, Hopf unstable, unstable and stable according to the linear analysis. In the left panel of Fig. 4, trajectories for the S, I, B populations are shown. The parameter setting is as in Example 2, Table 3, apart from the values $\beta = 1.76$, $\xi = 12.0203$. With these choice, the invariants for the endemic

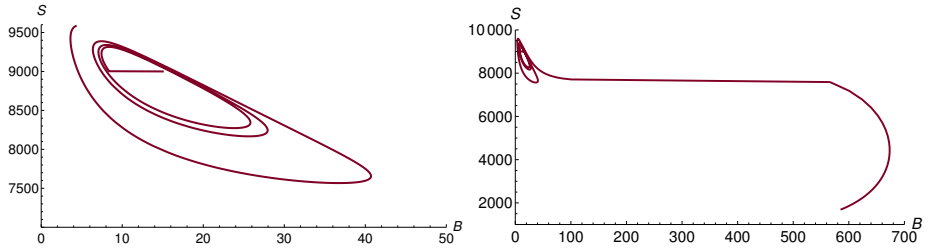

Figure 5. Phase plane portrait in the (B, S)-plane of the trajectories corresponding to the initial condition $(9000, 50, 15)$ in the parameter setting of Example 2 in Table 3, apart from β = 1.757, ξ= 12.03. With these choice, the endemic equilibrium $E_1 \approx (8916, 80, 14)$ is stable, but very close to the Hopf bifurcation limit. In the left panel, the orbit up to $T = 1500$, in the right panel, the complete path towards the other equilibrium value $E_{\rm up} \approx (1704, 615, 587)$.

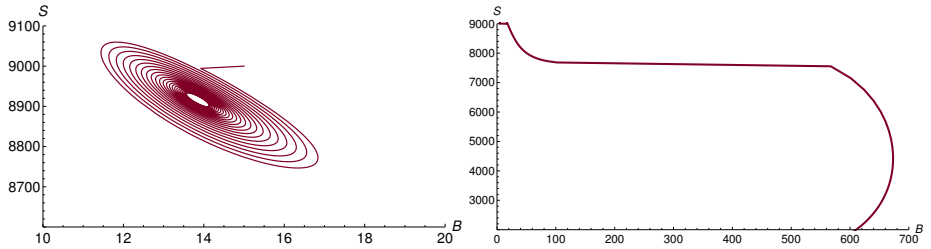

Figure 6. Phase plane portraits in the (B, S)-plane of the trajectories corresponding to the initial condition $S_0 = 9000$, $B_0 = 15$ in the parameter setting of Example 2 in Table 3, apart from $\beta = 1.757$, $\xi = 12.03$. With these choice, the endemic equilibrium $E_1 \approx (8916, 80, 14)$ is stable, but very close to the Hopf bifurcation limit. In the left panel, the orbit starting from $I_0 = 80$ and converging (very slowly, simulation is run until $T = 10000$) to E_1, in the right panel, the orbit starting from $I_0 = 30$ and more rapidly converging ($T = 2000$) to the other equilibrium value $E_{\rm up} \approx (1704, 615, 587)$.

equilibrium $E_1 \approx (8916, 80, 14)$ fulfill the conditions for the onset of a Hopf bifurcation. We also evaluate the related first Lyapunov coefficient l_1 by (35) and found a negative value, so that the Hopf bifurcation near the critical point E_1 is supercritical. However, our simulations are only able to show that the system trajectories, even starting very close to E_1, are attracted towards the stable endemic equilibrium $E_{\rm up} \approx (1704, 615, 587)$. To further explore this situation, we then consider a slight perturbation of the parameter values ($\beta = 1.757$, $\xi = 12.03$), so to move the equilibrium point E_1 just within the limits of its linear stability. Even in this case, reported in the right panel of the same figure, the process trajectories, after several oscillations, are eventually attracted by the upper branch equilibrium $E_{\rm up}$. Figure 5 helps clarify this latter situation by showing the corresponding phase portrait: up to $T = 1500$, the orbit remains quite close to E_1 (left panel of the figure), but the enlarging oscillations lead the process to converge to $E_{\rm up}$ (right panel of the same figure). Further investigations confirm that the lower branch equilibrium, even when it is stable, has a very small basin of attraction, and the system trajectories are highly sensitive to the chosen initial point: in Fig. 6, we report two phase plane portraits corresponding to the same equilibrium, in the same parameters setting, but with different initial values for the Infected population I_0. It can be clearly seen how the corresponding

orbits are dramatically different and eventually converge to different equilibrium values: E_1 (left panel) or E_{up} (right panel).

7.3 Experiments on sensitive parameters

It is clear that the stable endemic equilibrium with $\bar{B}$ greater than k_1, present in both scenarios, is heavily depending on the value of the carrying capacity k_1 that represents a lower bound for it. As discussed in the previous section, however, other parameters can play a significant role in the proposed model. Specifically, we further analyze the parameter setting of Example 2 and try to identify effective strategies to control the amplitude and timing of the peaks in both the infective and bacterial populations in the event of large $\mathcal{R}_0$ when the infectious disease spreads out and the only stable equilibrium in the considered model is the endemic one. In Fig. 7, we show trajectories of the Infected population obtained in the parameters setting of Example 2 when only one of the parameters values (β in the left panel, δ in the right one) is modified (increased or decreased) by 10%. These parameters characterize the main contributions to the infected population dynamics. As shown in the figure and as expected by the opposite sign of their contribution in the model, their fluctuations affect the timing of the Infected peak in opposite ways and cause a shift in the peak location without sensibly modifying the equilibrium value. However, changes in β values seem to have a greater impact moving further the peak location. A similar behavior can be observed in the bacterial dynamics (not shown).

To conclude this section, let us present, in the same experiment setting, the impact of different growth parameters r on the infected population. In Fig. 8, we represented the infected-population curves corresponding to several values of r ranging from 0 to 0.25. It is clear that the linear assumption for the pathogen growth ($r = 0$) corresponds to an abrupt growth of the infected population, while the nonlinear assumption allows to reproduce different scenarios, where the peak in the infected population could be lowered and shifted to the right to better fit experimental data. This could be the case for an epidemic spreading at different rates in different regions of the same country as reported in several experimental studies (see, i.e. [19]).

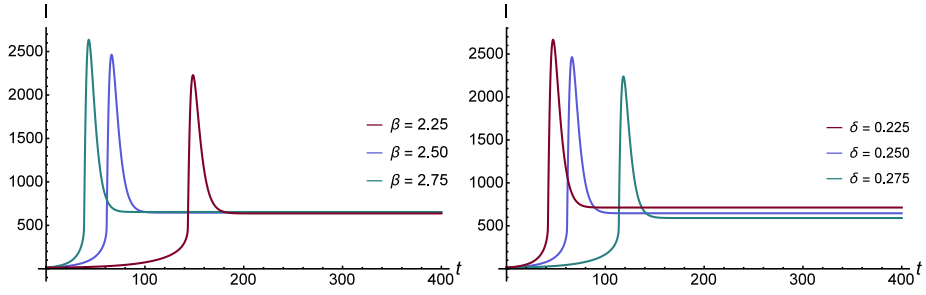

Figure 7. Model predictions for the Infected population with parameter values as in Example 2 of Table 3 (blue trajectory) and with an increase or decrease of 10% (green and red lines, respectively) of the parameters β (left panel) and δ (right panel).

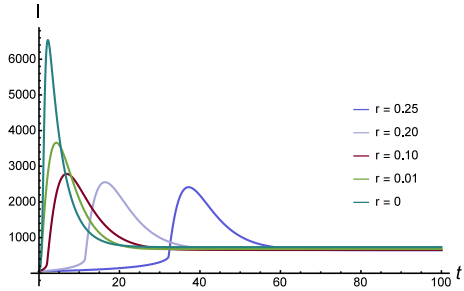

Figure 8. Model predictions for the infected populations with all parameter values as in Example 2 of Table 3 and different values of the r parameter ranging from 0 (dark green line) to 0.25 (blue line).

8 Conclusions

An ODEs model for the transmission of a waterborne disease has been formulated and investigated, both theoretically and numerically. Its main features are the cubic growth of the bacterial population, that implies an Allee effect, and a Holling type II functional response to better express the shape of the indirect transmission. For this model, the number of biologically meaning equilibria has been obtained along with their linear stability according to the basic reproduction number. The occurrence of a backward bifurcation has been investigated. Precisely, restrictions on the parameters guaranteeing the onset of a backward or a forward bifurcation, that can have consequences for the disease control, have been obtained. Hopf bifurcation has been analyzed by using methods from bifurcation theory and the center manifold theorem. Numerical simulations have confirmed the theoretical analysis and shown the rich dynamics in case of coexistence of two stable equilibria. A sensitivity analysis on $\mathcal{R}_0$ has been also performed to assess the incidence of the different parameters on the initial disease transmission. The obtained results could be a useful contribution to better understand and more realistically describe the dynamics of waterborne diseases. They could also be the starting point for giving insight to future studies aimed at planning intervention strategies.

Acknowledgment. The authors thank the anonymous referees for their suggestions, which have led to improvements in the manuscript.

References

1. N. Ashbolt, Microbial contamination of drinking water and disease outcomes in developing regions, *Toxicology*, **198**:229–238, 2004, https://doi.org/10.1016/j.tox.2004.01.030.

2. F. Capone, On the dynamics of predator-prey models with the Beddington–De Angelis functional response, under Robin boundary conditions, *Ric. Mat.*, **57**:137–157, 2008, https://doi.org/10.1007/s11587-008-0026-9.

3. F. Capone, M.F. Carfora, R. De Luca, I. Torcicollo, On the dynamics of an intraguild predator–prey model, *Math. Comput. Simul.*, **149**:17–31, 2018, https://doi.org/10.1016/j.matcom.2018.01.004.
4. F. Capone, M.F. Carfora, R. De Luca, I. Torcicollo, Turing patterns in a reaction–diffusion system modeling hunting cooperation, *Math. Comput. Simul.*, **165**:172–180, 2019, https://doi.org/10.1016/j.matcom.2019.03.010.
5. F. Capone, V. De Cataldis, R. De Luca, On the stability of a SEIR reaction diffusion model for infection under Neumann boundary conditions, *Acta Appl. Math.*, **132**:165–176, 2014, https://doi.org/10.1007/s10440-014-9899-7.
6. F. Capone, V. De Cataldis, R. De Luca, Influence of diffusion on the stability of equilibria in a reaction–diffusion system modeling cholera dynamic, *J. Math. Biol.*, **71**:1107–1131, 2015, https://doi.org/10.1007/s00285-014-0849-9.
7. M.F. Carfora, I. Torcicollo, Identification of epidemiological models: the case study of Yemen cholera outbreak, *Appl. Anal.*, 2020, https://doi.org/10.1080/00036811.2020.1738402.
8. C. Castillo-Chavez, B. Song, Dynamical models of tubercolosis and their applications, *Math. Biosci. Eng.*, **1**:361–404, 2004.
9. N. Chitnis, J.M. Hyman, J.M. Cushing, Determining important parameters in the spread of malaria through the sensitivity analysis of a mathematical model, *Bull. Math. Biol.*, **70**:1272–1296, 2008, https://doi.org/10.1007/s11538-008-9299-0.
10. C.T. Codeco, Endemic and epidemic dynamics of cholera: Yhe role of the aquatic reservoir, *BMC Infect. Dis.*, **1**:1, 2001, https://doi.org/10.1186/1471-2334-1-1.
11. O. Diekmann, J.A.P. Heesterbeek, J.A.J. Metz, On the definition and the computation of the basic reproduction ratio R_0 in models for infectious diseases in heterogeneous populations, *J. Math. Biol.*, **28**:365–382, 1990.
12. J.N. Eisenberg, M. Brookhart, G. Rice, M. Brown, J. Colford, Disease transmission models for public health decision making: Analysis of epidemic and endemic conditions caused by waterborne pathogens, *Environ. Health Persp.*, **110**:783–790, 2002, https://doi.org/10.1289/ehp.02110783.
13. Y.H. Grad, J.C. Miller, M. Lipsitch, Cholera modeling: Challenges to quantitative analysis and predicting the impact of interventions, *Epidemiology*, **23**:523–530, 2012, https://doi.org/10.1097/EDE.0b013e3182572581.
14. M.A. Jensen, S.M. Faruque, J.J. Mekalanos, B.R. Levin, Modeling the role of bacteriophage in the control of cholera outbreaks, *Proc. Natl. Acad. Sci. USA*, **103**(12):4652—4657, 2006, https://doi.org/10.1073/pnas.0600166103.
15. R.B. Kaul, A.M. Kramer, F.C. Dobbs, J.M. Drake, Experimental demonstration of an Allee effect in microbial populations, *Biol. Lett.*, **12**(4):20160070, 2016.
16. K. Levy, A.P. Woster, R.S. Goldstein, E.J. Carlton, Untangling the impacts of climate change on waterborne diseases: A systematic review of relationships between diarrheal diseases and temperature, rainfall, flooding, and drought, *Environ. Sci. Technol.*, **50**(10):4905–4922, 2016, https://doi.org/10.1021/acs.est.5b06186.
17. G. Lo Iacono, B. Armstrong, L.E. Fleming, R. Elson, S. Kovats, S. Vardoulakis, Challenges in developing methods for quantifying the effects of weather and climate on water-associated

diseases: A systematic review, *PLoS Negl. Trop. Dis.*, **11**:e0005659, 2017, https://doi.org/10.1371/journal.pntd.0005659.

18. D.R. Merkin, *Introduction to the Theory of Stability*, Texts Appl. Math., Vol. 24, Springer, New York, 1997.
19. Z. Mukandavire, S. Liao, J. Wang, H. Gaff, Estimating the reproductive numbers for the 2008–2009 cholera outbreak in Zimbabwe, *Proc. Natl. Acad. Sci. USA*, **108**:8767–72, 2011, https://doi.org/10.1073/pnas.1019712108.
20. R. Naresh, S. Pandey, A.K. Misra, Analysis analysis of a vaccination model for carrier dependent infectious diseases with environmental effects, *Nonlinear Analysis: Modelling and Control*, **13**(3):331–350, 2008.
21. H. Quan, X. Zhou, J. Liu, Global exponential stability of positive periodic solutions for a cholera model with saturated treatment, *Nonlinear Anal. Model. Control*, **23**(5):619–641, 2018.
22. S. Rionero, I. Torcicollo, Stability of a continuous reaction–diffusion Cournot–Kopel duopoly game model, *Acta Appl. Math.*, **132**:505–513, 2014, https://doi.org/10.1007/s10440-014-9932-x.
23. S. Rionero, I. Torcicollo, On the dynamics of a nonlinear reaction–diffusion duopoly model, *Int. J. Non-Linear Mech.*, **99**:105–111, 2018, https://doi.org/10.1016/j.ijnonlinmec.2017.11.005.
24. J.H. Tien, D.J. Earn, Multiple transmission pathways and disease dynamics in a waterborne pathogen model, *Bull. Math. Biol.*, **72**:1506–1533, 2010, https://doi.org/10.1007/s11538-010-9507-6.
25. I. Torcicollo, On the nonlinear stability of a continuous duopoly model with constant conjectural variation, *Int. J. Non-Linear Mech.*, **81**:268–273, 2016, https://doi.org/10.1016/j.ijnonlinmec.2016.01.018.
26. P. van der Driessche, Reproduction numbers and sub-threshold endemic equilibria for compartmental models of disease transmission, *Math. Biosci.*, **180**:29–48, 2002, https://doi.org/10.1016/S0025-5564(02)00108-6.
27. J. Wang, S. Liao, A generalized cholera model and epidemic–endemic analysis, *J. Biol. Dyn.*, **6**(2):568–589, 2012, https://doi.org/10.1080/17513758.2012.658089.
28. X. Wang, J. Wang, Analysis of cholera epidemics with bacterial growth and spatial movement, *J. Biol. Dyn.*, **9**:233–261, 2015, https://doi.org/10.1080/17513758.2014.974696.
29. C. Yang, J. Wang, On the intrinsic dynamics of bacteria in waterborne infections, *Math. Biosci.*, **296**:71–81, 2018, https://doi.org/10.1016/j.mbs.2017.12.005.